Case Study

Assessing the Effectiveness of Spreader Canals in Delivering Water to Marshes

David A. Chin, F.ASCE[1]; Patrick M. Kelly[2]; Russell T. Kiger[3]; and Roy S. Sonenshein[4]

Abstract: Hydrodynamic modeling is usually necessary for predicting water deliveries to marshes from source reservoirs. A novel approach is developed that decouples the delivery structure hydraulics from the marsh hydrodynamics, allowing these components to be analyzed both separately and in combination. This approach is applied to assess the effectiveness of incorporating spreader canals into water delivery systems in Everglades National Park. The results show that Manning's n in the marsh can be reasonably approximated as a function of VR, in which V is the flow velocity and R is the hydraulic radius; spreader canals can provide substantial percentage increases in water deliveries compared to the smaller structure tailwater pools, and spreader canal outflows can be linear functions of the length of the spreader canal. **DOI: 10.1061/(ASCE)HE.1943-5584.0000369.**

CE Database subject headings: Marshes; Hydraulic models; Canals; Hydraulic roughness; Water flow; Hydrodynamics; Reservoirs.

Author keywords: Marsh; Spreader; Model; Canal; Roughness; Flow.

Introduction

Water delivery to marshes is commonly done by using control structures, such as culverts or gated spillways, and such structures usually terminate in tailwater pools from which water overflows into the marsh. The downstream marsh areas can be either natural, in which case the preservation of functional wetlands is a concern, or engineered systems, such as treatment wetlands. An important issue from an engineering perspective is quantification of the extent to which the shape and dimensions of the delivery structure and tailwater pool affect water deliveries to the marsh area. Tailwater pools are usually small water bodies immediately downstream of delivery structures that primarily serve to dissipate excessive velocities that might erode the downstream marsh. In contrast, spreader canals are long dead-end channels that are hydraulically connected to the delivery structure and deliver water to a more extensive surrounding area by overflow. This is in contrast to other types of canals that deliver water to marshes through seepage into the underlying aquifer (e.g., Genereux and Slater 1999). In designing spreader canals, it is essential to be able to quantify the relationship between the spreader canal geometry and water delivery to the adjacent marsh area. Quantification of improvements in water deliveries when small tailwater pools are replaced by larger spreader canals also requires systemic consideration of the increased head losses that occur across the delivery structure as a result of increased flows and an assessment of the hydraulic impact of alternative structural modifications.

Field studies of the performance of spreader canals and guidelines for designing these canals are largely missing from the open technical literature. This paper describes a formal modeling procedure for predicting the performance of marsh spreader canals and relating the performance of these canals to the performance of the overall water delivery system that includes the delivery structure. The proposed protocol, which has field monitoring, hydraulic, and hydrodynamic modeling components, is demonstrated in this paper.

Methods

A typical spreader canal delivery system is shown in Fig. 1. At the upstream end of the system is a source reservoir, which is the headwater of the system. Connecting the source reservoir to the downstream spreader canal, or tailwater pool, is the delivery structure, which typically includes gated spillways, culverts, and bridges. Flow from the tailwater pool into the marsh will depend on the water stages in the marsh and the tailwater pool and the physical characteristics of the marsh and tailwater pool.

Steady-state flow within marshes can be described by the depth-integrated continuity and momentum equations given, respectively:

$$h\left(\frac{\partial u}{\partial x}+\frac{\partial v}{\partial y}\right)+u\frac{\partial h}{\partial x}+v\frac{\partial h}{\partial y}=0 \tag{1}$$

$$hu\frac{\partial u}{\partial x}+hv\frac{\partial u}{\partial y}-\frac{h}{\rho}\left[E_{xx}\frac{\partial^2 u}{\partial x^2}+E_{xy}\frac{\partial^2 u}{\partial y^2}\right]+gh\left[\frac{\partial a}{\partial x}+\frac{\partial h}{\partial x}\right]+\frac{gun^2}{(h^{1/6})^2}(u^2+v^2)^{1/2}=0 \tag{2}$$

$$hu\frac{\partial v}{\partial x}+hv\frac{\partial v}{\partial y}-\frac{h}{\rho}\left[E_{yx}\frac{\partial^2 v}{\partial x^2}+E_{yy}\frac{\partial^2 v}{\partial y^2}\right]+gh\left[\frac{\partial a}{\partial y}+\frac{\partial h}{\partial y}\right]+\frac{gun^2}{(h^{1/6})^2}(u^2+v^2)^{1/2}=0 \tag{3}$$

[1]Professor, Dept. of Civil Engineering, Univ. of Miami, Coral Gables, FL 33146 (corresponding author). E-mail: dchin@miami.edu

[2]Graduate Student, Dept. of Civil Engineering, Univ. of Miami, Coral Gables, FL 33146.

[3]Graduate Student, Dept. of Civil Engineering, Univ. of Miami, Coral Gables, FL 33146.

[4]Hydrologist, Everglades National Park, South Florida Ecosystem Office, Homestead, FL 33030.

Note. This manuscript was submitted on January 17, 2010; approved on December 29, 2010; published online on January 3, 2011. Discussion period open until March 1, 2012; separate discussions must be submitted for individual papers. This paper is part of the ***Journal of Hydrologic Engineering***, Vol. 16, No. 10, October 1, 2011. ©ASCE, ISSN 1084-0699/2011/10-829–836/$25.00.

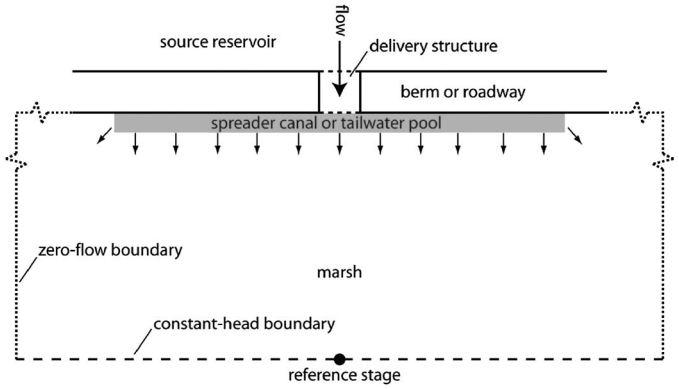

Fig. 1. Typical system for delivering water to marshes

in which h = the water depth; u and v = the velocities in the Cartesian directions x and y, respectively; t = time; ρ is the density of water; E_{xx}, E_{yy}, E_{xy}, and E_{yx} = the components of the eddy viscosity tensor; g = gravity; a = the elevation of the bottom of the marsh; and n = the Manning roughness coefficient. The momentum equations [Eqs. (2) and (3)] neglect the influence of wind on marsh flow because the emergent marsh vegetation largely protects the water from wind effects, and hence, the marsh flow is primarily driven by gravity. In conventional hydrodynamic modeling of the marsh flow, Eqs. (1)–(3) are solved for given boundary and initial conditions by using computer codes such as RMA-2 [U.S. Army Corps of Engineers (USACE) 2008] and FESWMS (Froehlich 2002), although other models and formulations could also be used (e.g., Hammer and Kadlec 1986). However, these models are limited in that users must either construct detailed finite-element meshes to describe flow through the delivery structure or specify structure rating curves in a fixed functional form that might not apply to all feasible structures. For example, the RMA-2 code cannot explicitly accommodate delivery structures with rating curves in which the flow through the structure depends on both the headwater and tailwater elevation, such as might occur under some culvert flow conditions. Because the strength of conventional computer codes is in simulating the marsh hydrodynamics under complex flow conditions, a novel modeling approach for water delivery to marshes is presented here that decouples the simulation of marsh hydrodynamics from the structure hydraulics and then explicitly combines the results of these submodels to describe the complete water delivery process. The proposed method requires the separate determination of performance curves for both the delivery structure and the marsh.

The performance curve for a delivery structure relates the flow, Q, through the structure to the headwater stage, z_H, and the tailwater stage, z_T, and this relationship can be put in the functional form

$$z_H = f_S(z_T|Q) \tag{4}$$

in which the function f_S depends on the characteristics of the structure. This performance curve can be determined by either field measurements or estimated theoretically for various flow regimes by using a hydraulic model of the structure. Steady-state flow through the marsh is governed by the continuity and momentum equations given by Eqs. (1)–(3), and typical boundary conditions for these equations are illustrated in Fig. 1. At the upstream boundary of the marsh flow domain, a constant inflow rate is specified for the boundary segment containing the delivery structure with a zero-flux boundary condition along the remainder of the upstream boundary. The zero-flux condition on the upstream boundary is typically a consequence of a berm or elevated roadway along this boundary. Under usual conditions, the lateral boundaries are also zero-flux boundaries, either because of constraining berms or symmetry with flows from adjacent delivery structures. At the downstream end of the marsh domain is a constant-head boundary that defines the water stage in the marsh. The downstream constant-stage boundary condition forces the flow to be normal to the upstream boundary, and so, the downstream boundary must be sufficiently far downstream that lateral velocities induced by the spreader canals are much smaller than the longitudinal velocities. For marshes with a known topography, specified inflow at the upstream boundary (from the tailwater pool) and specified stage on the downstream boundary, model calibration consists of varying the Manning roughness within the marsh until the stage on the upstream boundary calculated by the steady-state hydrodynamic model [Eqs. (1)–(3)] matches the measured stage corresponding to the specified marsh inflow and the specified downstream stage. Once calibrated, the model results for marsh flow can be expressed in the form

$$z_T = f_M(Q|z_M) \tag{5}$$

in which z_T = the stage in the tailwater pool (at the upstream end of the marsh); z_M = stage at the downstream end of the marsh; Q = the marsh inflow; and the function f_M depends on the physical characteristics of both the marsh and tailwater pool. The relationship given by Eq. (5) will be referred to in this paper as the marsh performance curve, although it could also appropriately be called the marsh backwater curve. Combining Eqs. (4) and (5) gives the overall performance of the water delivery system as

$$z_H = f_S(f_M(Q|z_M)|z_M) = f_{SM}(Q|z_M) \tag{6}$$

in which the water delivery function, f_{SM}, relates the headwater stage, z_H, to the flow delivery, Q, for a given marsh stage, z_M, and is derived from the two canonical functions, f_S and f_M, which can be determined separately from the structure performance curve and marsh performance curve, respectively. The functional relationship given by Eq. (6) is particularly appealing because it isolates the impact of modifications to the tailwater pool on water deliveries from the impact of structural modifications on water deliveries. In cases in which only the tailwater pool is modified, the delivery structure performance curve remains unchanged and only the marsh performance curve needs to be modified to account for changes in marsh hydrodynamics. In cases in which the delivery structure is modified, only the structure performance curve needs to be modified, and no additional hydrodynamic modeling is necessary. Tailwater pool modifications, such as increasing the perimeter of the pool that is in contact with the marsh, and structural modifications, such as increasing the dimensions of openings and other modifications to reduce head losses at structures, can be easily considered.

This paper describes an application of the proposed methodology to assess the impact on water delivery resulting from increasing the size of tailwater pools into so-called spreader canals and isolates the impact of structural modifications on these water deliveries. Two supporting issues that are also addressed are (1) identification of field measurements that are necessary to support calibration of the marsh hydrodynamic model and (2) an assessment of the extent to which modifications in the tailwater pool impact the calibration parameters of the marsh hydrodynamic model.

Field Study

The proposed method was applied to predict the impact of replacing existing tailwater pools of culvert delivery structures with spreader canals in Everglades National Park (ENP) in Florida.

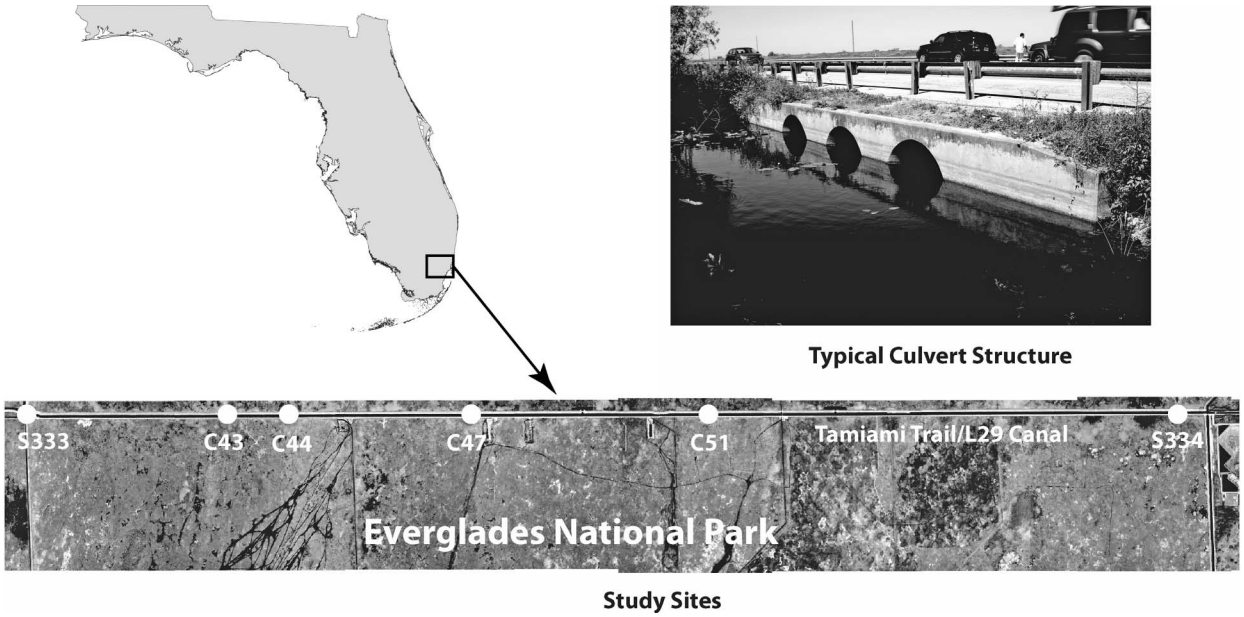

Fig. 2. Locations of study sites (aerial photography from USGS Map Server, May 2009)

The northern boundary of ENP includes a 17.2 km section of the US41 roadway commonly known as Tamiami Trail where water is delivered to ENP by several three-barrel culvert structures as shown in Fig. 2. The source of the water is the L29 canal on the north side of Tamiami Trail, and stages within the L29 canal are controlled by gated spillways (S333 and S334) at the western and eastern ends of the canal. The water delivery structures of interest in this study are the culverts designated as C43 and C51, and a typical tailwater view of one of these structures is shown in Fig. 2. Under existing conditions, stages in the L29 canal are regulated so as not to exceed a maximum stage of 1.83 m relative to the North American Vertical Datum of 1988 (NAVD88), and this datum is used for all elevations given in this paper. The culvert structures have existing tailwater pools with approximate dimensions ($L \times W$) of 22 m × 14 m at C43 and 15 m × 14 m at C51. It has been proposed that increased water deliveries from L29 into ENP can be achieved by replacing the existing tailwater pools with spreader canals. The spreader canal dimensions under consideration here are 152 m × 9 m, 305 m × 9 m, and 457 m × 9 m, in which the long side of the spreader canals would run adjacent to the Tamiami Trail roadway. Application of the proposed modeling approach is shown in detail for the C43 site, and the key results are presented for both the C43 and C51 sites to illustrate the variety of outcomes that can be achieved at different sites.

Marsh Model

The boundaries of the marsh hydrodynamic model at the C43 site are shown in Fig. 3. The upstream (northern) boundary of the hydrodynamic model is defined by the Tamiami Trail roadway, the western boundary is midway between C43 and an adjacent similar delivery structure to the west (C42), the downstream boundary is approximately 400 m downstream of the northern boundary, and the eastern boundary coincides with an elevated secondary roadway that will constrain the flow. The topography of the marsh within the model domain was measured by using global positioning system

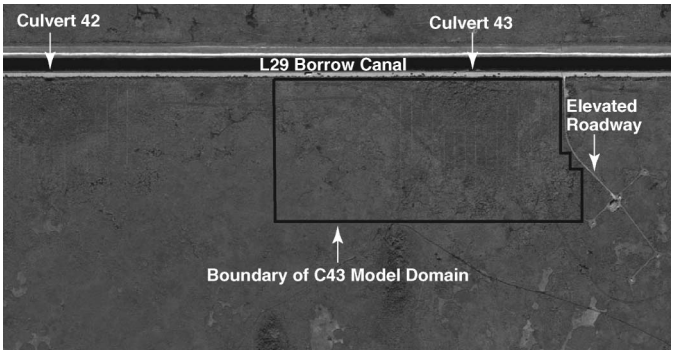

Fig. 3. C43 study site (aerial photography from USGS Map Server, May 2009)

real-time kinematic (GPS RTK) instrumentation along north-south transects, in which the transects were 30.5 m apart, and measurements were taken at 6.1 m intervals along each transect. A *halo* of dense exotic vegetation surrounds the tailwater pool, and the extent of this halo was estimated from the color versions of aerial photographs shown in Fig. 3. The delineated halo area, which contains primarily woody vegetation, was assumed to have significantly different roughness characteristics than the marsh area downstream of the halo that contains primarily sawgrass. The RMA-2 finite-element computer code (USACE 2008) was used to develop the marsh hydrodynamic model. The dimensions of the rectangular finite elements in the model downstream of the tailwater pool were specified as 30.5 m × 12.2 m so that the mesh nodes coincided with measurement locations, which minimized any errors associated with spatial interpolation of marsh topography within the mesh. In accordance with guidance provided by USACE (2008), eddy viscosities were specified automatically within the model to maintain an element Peclet number of 20, in which the Peclet number (Pe) is given by

$$\mathrm{Pe} = \frac{\rho V \Delta}{E} \tag{7}$$

in which E = component of the eddy viscosity tensor in the flow direction (the transverse component of the eddy viscosity relative to the flow direction is assumed as zero); V = flow velocity in the element; and Δ = length of the element in the flow direction. The marsh porosity algorithm within the RMA−2 model was used to account for subgrid topographic variations and partial drying within finite elements (Hayashi and van der Kamp 2000); however, the interior of the marsh did not generally go dry for any of the scenarios reported in this paper.

Field Measurements

For approximately four months before model construction, flows through the upstream culvert structures that deliver water to the marsh area were recorded at 15 min intervals by using Argonaut-SW (SonTek, Inc.) acoustic Doppler current profilers (ADCPs) fixed to the bottom of the center barrel of each culvert structure, with the total flow through the three-barrel structure estimated as three times the flow in the center barrel. During the same monitoring period, synoptic stages were measured in the tailwater pool immediately downstream of each culvert structure and in the marsh at the downstream end of the model boundary. All stages were measured by using HOBO (Onset Computer Corp.) pressure transducers mounted in stilling wells, and all stages were recorded at the same times as the flow measurements.

The marsh performance curves derived from the stage and flow measurements are shown as solid lines in Fig. 4 for marsh stages, z_M, of 1.77 and 1.74 m. In accordance with Eq. (4), the marsh performance curves are plots of pool elevation, z_T, as a function of the flow rate, Q, for given values of the marsh stage, z_M. It is apparent from Fig. 4 that a linear approximation of the measured data is appropriate for cases in which the stage in the tailwater pool exceeds the marsh stage, in which the performance curves are estimated by visual approximation. A tolerance of ± 0.015 m was allowed for the nominal marsh stages of 1.77 and 1.74 m, and for tailwater pool stages greater than the marsh stage, flows are positive and into the marsh from the tailwater pool, whereas for tailwater pool stages less than the marsh stage, flows are negative and out of the marsh into the tailwater pool. When pool stages are close to the marsh stage, there exists some variability in the results introduced by the stage tolerance because the actual marsh stage could be greater than the pool stage even though the nominal marsh stage is less than the pool stage.

Calibration of Marsh Model

The only calibration parameter in the marsh hydrodynamic model is the Manning roughness, and this parameter is adjusted in the model until the model output accurately reproduces the selected points on the measured marsh performance curve shown in Fig. 4. The first step in calibrating the marsh model is to identify target points on the measured marsh performance curve that are to be reproduced exactly by the marsh hydrodynamic model of existing conditions. These target points are shown in Fig. 4 and are defined as the pool stages corresponding to flows of 0.14 m^3/s, 0.28 m^3/s, 0.42 m^3/s, and 0.57 m^3/s for downstream marsh stages of 1.77 and 1.74 m. The specified inflows and the corresponding downstream marsh stages were input into the marsh hydrodynamic model, and the values of Manning's n that yield the corresponding

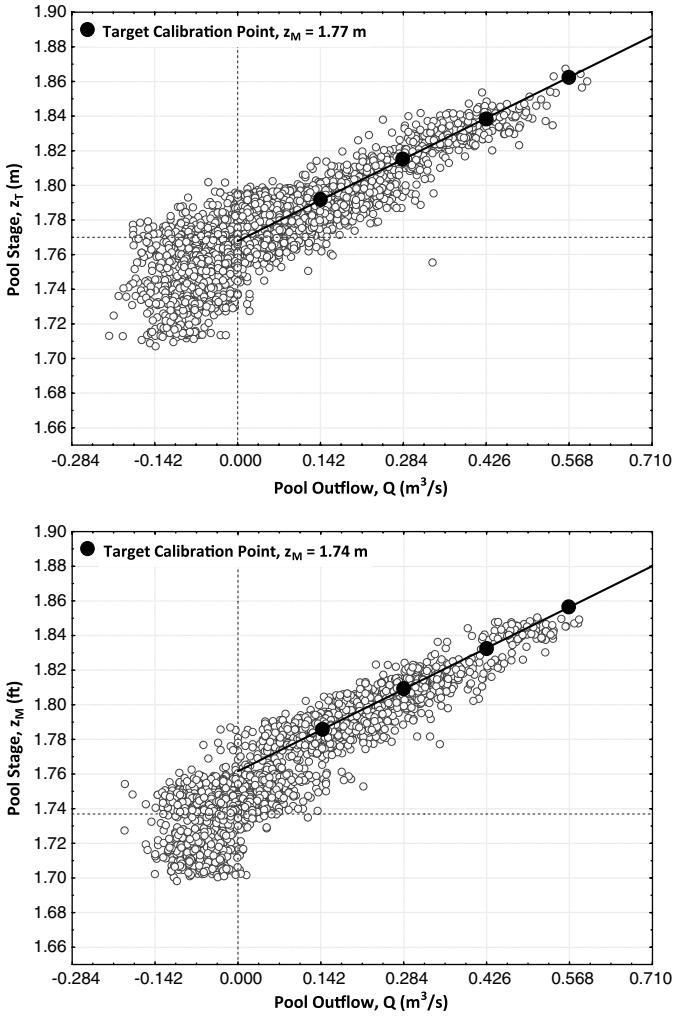

Fig. 4. Measured marsh performance curves

(observed) tailwater pool elevations were determined for each target point.

Numerous studies reported in the technical literature have confirmed that the Manning roughness in marshes cannot be assumed as a constant that is independent of the flow condition and local vegetation density (Tsihrintzis and Madiedo 2000; Kadlec 1990). Furthermore, flow conditions in marshes are usually not fully turbulent and so, by analogy to classical friction-factor analysis, Manning's n must be assumed as a function of both the flow Reynolds number and ratio of flow depth to a characteristic marsh roughness height (Chin 2006). Assuming that a fixed and site-specific marsh roughness height reflects the type of marsh vegetation, the Manning's n for any particular marsh can be assumed as a function of the Reynolds number and the flow depth. The Reynolds number in marshes and grassed channels is conventionally measured by VR, in which V is the mean flow velocity and R is the hydraulic radius. Therefore, under general circumstances, n is a function of both VR and the flow depth, h. Many previous studies have indicated that n can be expressed entirely as a function of VR, and additional explicit h dependence can be neglected (Tsihrintzis and Madiedo 2000). In contrast, some applications express n entirely as a function of h, in which n is inversely proportional to h. In reality, both approaches can be justified because VR is a function of h.

Marsh conditions at the study site are complicated by the fact that there exist two vegetation zones in the marsh where the

Manning roughness is expected to be significantly different: the halo area immediately downstream of the tailwater pool, and the marsh area downstream of the halo. The marsh hydrodynamic model indicates that the higher velocities in the vicinity of the tailwater pool cause the majority of energy losses and stage attenuation to occur within the halo, and negligible head losses and stage differences occur between the halo and the downstream boundary of the model. This prediction was confirmed by stage measurements at several intermediate locations between the tailwater pool and the downstream boundary. As a consequence, the predicted flows into the marsh were insensitive to the roughness of the marsh area downstream of the halo, and the flows were only sensitive to the halo roughness. This sensitivity analysis was done by first calibrating the marsh hydrodynamic model for a uniform roughness (same in the halo and marsh areas) and then recalibrating the model by specifying the marsh roughness to be twice the halo roughness and again recalibrating the model by specifying the marsh roughness to be one half the halo roughness. Results showed that the calibrated halo roughness did not differ by more than 5% for any of the marsh roughness conditions considered.

Because most of the stage attenuation occurs immediately downstream of the tailwater pool and is controlled by the halo roughness, the $n - VR$ function derived from calibration of the marsh hydrodynamic model was identified as characterizing n in the halo for VR in the area immediately downstream of the tailwater pool. If the outflow from the tailwater pool is Q, the outflow perimeter is P, and the depth of flow immediately downstream of the tailwater pool is h_T, then VR can be estimated by

$$VR \approx \left(\frac{Q}{Ph_T}\right)(h_T) = \frac{Q}{P} \tag{8}$$

in which VR is approximately equal to the pool outflow divided by the outflow perimeter. By using Eq. (8) to calculate VR and a measured outflow perimeter of 49.4 m for the tailwater pool at C43, the Manning's n values derived from calibration are expressed as a function of VR in Fig. 5. Also shown in Fig. 5 are comparative roughness functions for sparse and dense marshes suggested by Tsihrintzis and Madiedo (2000) and the $n - VR$ function derived from model calibration at the C51 site. These results show that the derived $n - VR$ functions are consistent with previous results (Tsihrintzis and Madiedo 2000) and that the $n - VR$ functions are significantly different between the two research sites. This variability in the $n - VR$ function between sites is particularly noteworthy because it demonstrates that the $n - VR$ relationship can be very site-specific, even though the two research sites appear superficially very similar in the roughness characteristics of the halo and downstream marsh. These results collectively indicate that local measurements of the marsh performance function are essential in establishing $n - VR$ functions that are to be subsequently used in predicting the performance of spreader canals. The values of n found in this study are consistent with those found in previous investigations in ENP; specifically, n values in the range of 0.26 to 0.61 were reported by Swain et al. (2004), and values of n in the range of 0.45 to 0.55 were reported by Wang et al. (2007). Variano et al. (2009) conducted tracer studies in the Everglades water conservation areas (dominated by ridges and sloughs) north of the project area and reported that the Reynolds numbers were in the range of 450 to 920, indicating transitional flow, in which case Manning's n must be assumed as a function of the flow condition.

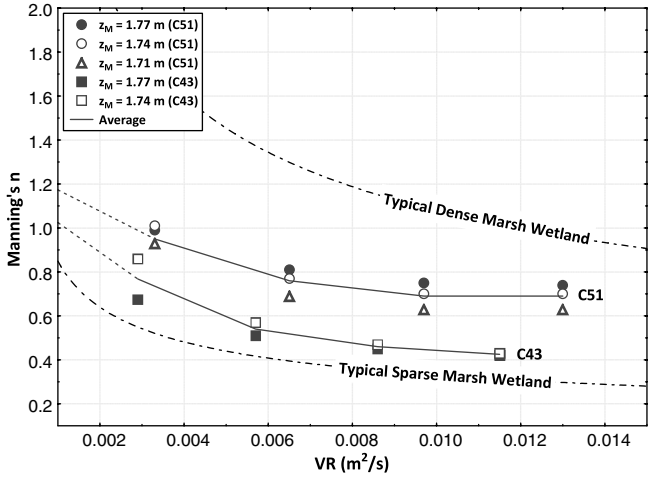

Fig. 5. Manning's n functions derived from model calibrations

Tailwater Pool Modifications

Marsh hydrodynamic models incorporating spreader canals were derived from the model of existing conditions incorporating the tailwater pool by simply adjusting the mesh to replace the tailwater pool by the spreader canal. An illustration of the mesh adjustment is shown in Fig. 6, where it is apparent that the mesh outside the immediate vicinity of the tailwater pool and spreader canal remains unchanged. For any given spreader canal outflow, the roughness of the halo and marsh areas are specified by using the $n - VR$ function extracted from the marsh hydrodynamic model under existing conditions. In the case of the spreader canal, VR is calculated by using Eq. (8) for the spreader canal outflow, Q, and spreader canal outflow perimeter, P. After mesh adjustment to accommodate the spreader canal, the hydrodynamic model with n determined from the $n - VR$ function was run for given values of inflow, Q, and marsh stage, z_M, and the resulting spreader canal stage, z_T, calculated by the hydrodynamic model. The resulting marsh

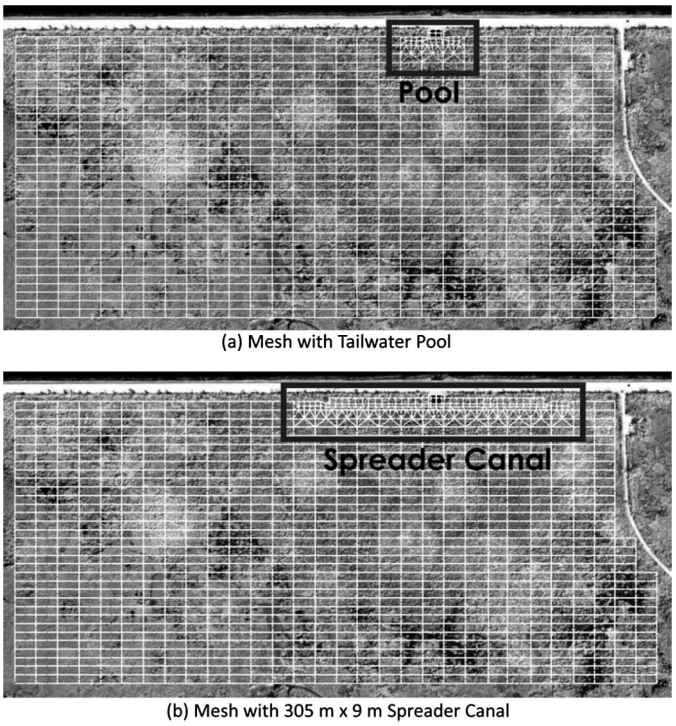

Fig. 6. Meshes used in hydrodynamic models (images courtesy of U.S. Geological Survey)

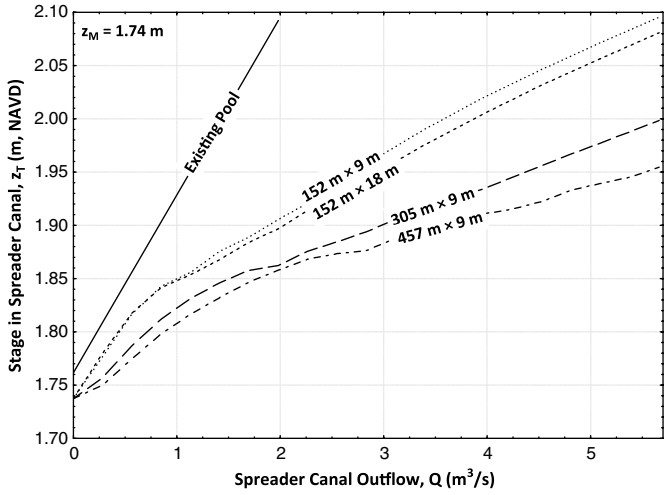

Fig. 7. Marsh performance curves derived from hydrodynamic models

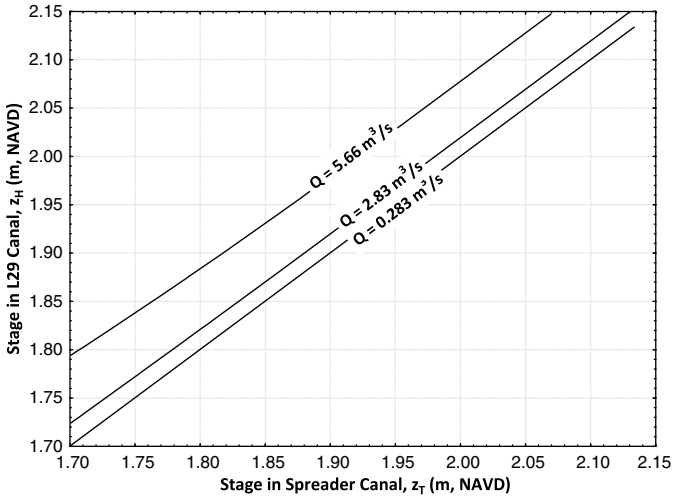

Fig. 8. Culvert structure performance curves

performance curves for C43 are shown in Fig. 7 for a nominal marsh elevation of 1.74 m. The calculated performance curves in Fig. 7 specify the functional relationship described by Eq. (5) and provide a clear indication of the increased flows relative to existing tailwater pools that will result from spreader canals of various dimensions. A notable feature in Fig. 7 is the linearity of the tailwater pool/marsh performance curve compared with the nonlinearity of the spreader canal/marsh performance curves. Whereas the linearity of the tailwater pool/marsh performance curve is a direct consequence of calibration to match field observations under existing conditions, the nonlinearity of the spreader canal/marsh performance curve reflects the controlling influence of topography at the spreader canal/marsh interface, which are considerably different between the existing tailwater pool and the proposed spreader canals.

The spreader canal/marsh performance function shown in Fig. 7 does not give the overall increase in water delivery that is of interest because it is the relationship between the headwater of the delivery structure and the flow into the marsh that is of concern. Therefore, in accordance with Eq. (6), the increased stage differences across the delivery structure that will result from increased flows associated with the spreader canal must be taken into account. These increased stage differences across the delivery structure will reduce some of the water delivery advantage of spreader canals over the existing tailwater pools. To account for head losses across a delivery structure, the performance curve of the structure must be known and expressed in the form of Eq. (4). In the present study, the delivery structures consist of three-barrel culverts. The performance curves for these structures were calculated by using direct-step backwater computations for partially full conditions and the Manning equation for full-flow conditions as described in Brunner (2002) (and incorporated in the widely used HEC-RAS code), in which a Manning n of 0.013 and an entrance loss of $0.2V_o^2/2g$ were assumed, in which V_o is the velocity at the entrance to a culvert barrel. The diameter of the concrete-lined culvert barrel is 1,520 mm, and the corresponding performance curve of the culvert structure is shown in Fig. 8. It is apparent from this performance function that for flow deliveries less than 0.28 m^3/s there exists negligible stage attenuation across the delivery structure. However, as the flow through the structure increases, the stage difference across the structure also increases.

Combining the marsh performance curves with the delivery structure performance curves in accordance with Eq. (6) gives the final water-delivery curves shown in Fig. 9, which correspond to a downstream marsh elevation of 1.74 m. The relationships shown in Fig. 9 are the primary bases for assessing the relative benefits of various spreader-canal configurations. Because operating rules for the upstream water source (the L29 canal) limit the maximum headwater elevation to 1.83 m, a headwater elevation of 1.83 m provides the benchmark for comparing the performances of the various spreader canal configurations with the existing tailwater pool. These comparative operating points are shown in Fig. 9 and are listed in Table 1. It is apparent that at the two sites studied, significant percentage increases in flow deliveries can be achieved by the use of spreader canals. For the spreader canals with dimensions of 152 m × 9 m, 305 m × 9 m, and 457 m × 9 m, flow increases of approximately 60, 150, and 200%, respectively, are expected at the C43 site. At the C51 site, corresponding flow increases are 250, 460, and 560%. A comparison of the flow deliveries for various lengths of the spreader canal at the C43 site is shown in Fig. 10. It is apparent that the flow delivered is linearly proportional to the length of the spreader canal. This linear relationship could be particularly important in performing benefit-cost analyses for different lengths of spreader canal.

The most critical assumption in deriving the spreader canal performance curves, and subsequently the water delivery curves, was

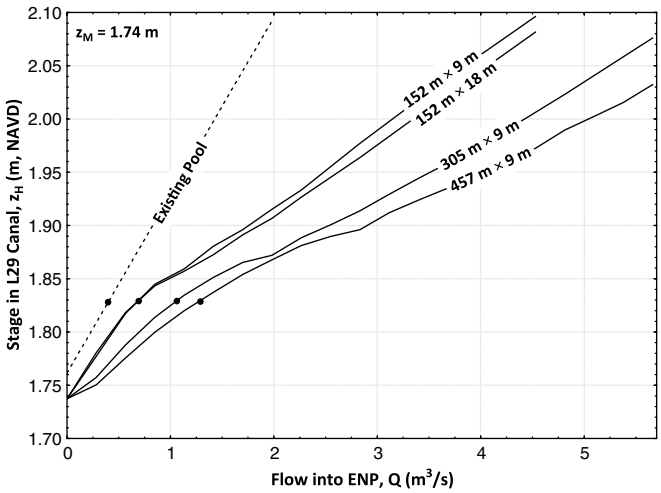

Fig. 9. Overall delivery system performance curves

Table 1. Flow Deliveries for Different Spreader Canal Configurations

Site	Marsh elevation z_M (m)	Flow into Everglades National Park (m^3/s)			
		Existing pool	152 m × 9 m spreader canal	305 m × 9 m spreader canal	457 m × 9 m spreader canal
C43	1.77	0.34	0.49	0.78	0.93
	1.74	0.36	0.62	0.96	1.16
C51	1.77	0.18	0.67	1.06	1.24
	1.74	0.23	0.78	1.27	1.47
	1.71	0.28	0.88	1.40	1.66

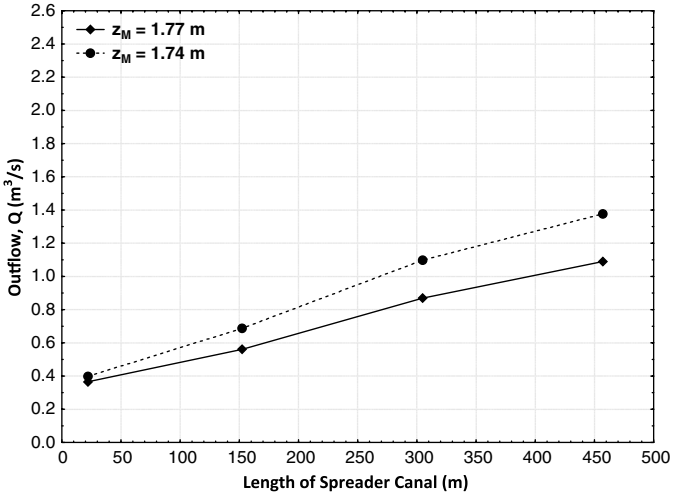

Fig. 10. Water delivery as a function of the length of spreader canal

the assumption that Manning's n is the same in both the halo and marsh areas. This assumption was necessary because stage attenuation downstream of the existing tailwater pools is dominated by the halo roughness, and so only the halo roughness could be reliably derived from field measurements. To determine the influence of this assumption on the estimated water deliveries given in Table 1, these water deliveries were recalculated by specifying the marsh roughness as equal to twice the halo roughness and also by specifying the marsh roughness as equal to one-half the halo roughness. The results of these calculations show that water deliveries are significantly increased if the marsh roughness is one half the halo roughness and are significantly decreased if the marsh roughness is twice the halo roughness. Specifically, for the 305 m × 9 m spreader canal at the C43 site, the uniform Manning n assumption predicts an increase of 150% in flow delivery relative to the existing tailwater pool, whereas increases of 37 to 250% are expected for marsh roughness varying from twice to one half the halo roughness, respectively. At the C51 site, the uniform Manning n assumption predicts an increase of 460% in flow delivery relative to the existing tailwater pool, whereas increases of 160 to 740% are expected for marsh roughness varying from twice to one-half the halo roughness.

A second consideration regarding the results in Table 1 is whether modifications to the delivery structure will improve water deliveries to the marsh area. From a hydraulic viewpoint, if head losses across the structure are small for the range of flow rates expected, then structural modifications will not have any significant effect on water deliveries. In the protocol presented in this paper, the structure performance curve is separate from the marsh performance curve, and so the impact of structural modifications can be easily assessed without having to reconsider the marsh

Table 2. Flow Deliveries from 457 m × 9 m Spreader Canal for Different Structures

Site	Marsh elevation z_M (m)	Flow into Everglades National Park (m^3/s)		
		Existing culvert 3-barrels	New culvert 6-barrels	Bridge
C43	1.77	0.93	0.98	0.98
	1.74	1.16	1.22	1.22
C51	1.77	1.24	1.42	1.53
	1.74	1.47	1.71	1.84
	1.71	1.66	1.91	2.04

hydrodynamics. In the present case, the effects of adding three additional barrels to the culvert structure was assessed by modifying the structure performance curve reducing the flow in the existing barrels by one half for the same headwater and tailwater stages. The effect of replacing the culvert structure by an ungated bridge was assessed by putting the headwater equal to the tailwater for all flows. The results of these modifications to the structure performance curve for the 457 m × 9 m spreader canal are shown in Table 2. These results indicate that flow increases at C43 with either structural modification will be minimal, whereas structural modifications at C51 will have a greater effect. This latter result is a consequence of the existing barrel diameters at C51 that are much smaller than those at C43 (1,220 mm versus 1,520 mm). Because the 457 m × 9 m spreader canal produces the highest flow deliveries of all the spreader canals considered, the advantages of structural modification are greatest for this spreader canal configuration and provide a limiting condition for the advantages of structural modifications with other spreader canal configurations.

Summary and Conclusions

A procedure for quantifying the increased water deliveries that could be achieved by replacing small tailwater pools by spreader canals in systems that deliver water to marshes from upstream reservoirs is proposed and demonstrated. In contrast to most existing approaches in similar situations, the proposed approach decouples the delivery structure performance from the marsh performance, allowing the contributions of these components to be analyzed separately. The marsh performance function introduces a new concept in which the steady-state flow through the marsh is characterized as a function of upstream and downstream stages. This marsh performance function is essentially the same as the marsh backwater curve in which two-dimensional flow in the marsh is taken into account. The determination of the marsh performance function under existing conditions is the focus of field measurements and is the basis for calibrating a steady-state marsh hydrodynamic model that reproduces the observed marsh performance function. The key outcome of this calibration process is the determination of

the Manning's n roughness function that relates n to the flow characteristics in the marsh. The spreader canal performance is then determined by replacing the existing marsh tailwater pool by a spreader canal in the marsh hydrodynamic model, by using the calibrated n-function to characterize the roughness.

The practicality of the proposed protocol is demonstrated on the northern boundary of ENP in Florida. Approximately linear tailwater pool/marsh performance curves were obtained from synoptic measurement of flow and stages at the upstream and downstream ends of the marsh. By using the measured marsh performance curves to calibrate steady-state marsh hydrodynamic models, it is shown that Manning's n can be adequately approximated as a function of VR, in which V is the flow velocity and R is the hydraulic radius. The derived $n - VR$ function is significantly different between the study sites; however, both $n - VR$ functions are consistent with previously reported $n - VR$ functions in both dense and sparse marshes. Applying the derived $n - VR$ functions in the marsh hydrodynamic models for several spreader canal configurations showed that spreader canals can provide substantial percentage increases in water deliveries compared with the smaller tailwater pools. It is further shown that spreader canal outflows can be a linear function of the length of the canal.

Because the structure and marsh performance curves are decoupled, the effect of structural modifications on water deliveries can be easily assessed without having to rerun any of the marsh hydrodynamic models. Under the best-case scenario, a delivery structure can be replaced by one in which there exists negligible head loss in the structure for the range of flows expected, and this would serve as a benchmark for considering other structural modifications to improve water deliveries to the marsh.

Overall, the results of this study show that the proposed protocol for predicting water deliveries to marshes by using spreader canals instead of smaller tailwater pools provides a practical approach that effectively combines field measurements with hydrodynamic modeling. Further insight on the performance of spreader canals could be gained by considering additional marsh and delivery structure configurations. Application of the proposed approach yields quantitative results that can be used as bases for making decisions on spreader canal utilization and sizing, and for assessing structural modifications that will further increase water deliveries to marsh areas.

Acknowledgments

This study was funded under task agreement number No. J5297-09-0053 between the National Park Service and the University of Miami.

Notation

The following symbols are used in this paper:

a = bottom elevation of marsh;
E = component of eddy viscosity tensor in flow direction;
E_{xx}, E_{yy}, E_{zz} = eddy viscosity coefficients in x, y, and z directions, respectively;
f_S = function defining delivery structure performance;
f_M = function defining marsh performance;
f_{SM} = function defining combined delivery structure and marsh performance;
g = gravity;
h = water depth;
h_T = flow depth immediately downstream of tailwater pool;
n = Manning roughness coefficient;
P = wetted perimeter of flow;
Q = volumetric flow rate into marsh;
R = hydraulic radius;
u = x-component of flow velocity;
v = y-component of flow velocity;
t = time;
V = magnitude of flow velocity;
x = Cartesian coordinate direction;
y = Cartesian coordinate direction;
z_H = headwater stage at delivery structure;
z_M = marsh stage at downstream end of study area;
z_T = tailwater stage at delivery structure;
Δ = length of finite element in streamwise direction; and
ρ = density of water.

References

Brunner, G. (2002). *HEC-RAS river analysis system hydraulics reference manual*, U.S. Army Corps of Engineers, Hydrologic Engineering Center, Davis, CA.

Chin, D. (2006). *Water-resources engineering*, 2nd Ed., Prentice-Hall, Upper Saddle River, NJ.

Froehlich, D. (2002). "User's manual for FESWMS FlO2-DH, release 3." *Publication No. FHWA-RD-03-053*, U.S. Federal Highway Administration, Washington, DC.

Genereux, D., and Slater, E. (1999). "Water exchange between canals and surrounding aquifer and wetlands in the southern Everglades, USA." *J. Hydrol. (Amsterdam)*, 219, 153–168.

Hammer, D., and Kadlec, R. (1986). "A model for wetland surface water dynamics." *Water Resour. Res.*, 22(13), 1951–1958.

Hayashi, M., and van der Kamp, G. (2000). "Simple equations to represent the volume-area-depth relations of shallow wetlands in small topographic depressions." *J. Hydrol. (Amsterdam)*, 237, 74–85.

Kadlec, R. (1990). "Overland flow in wetlands: Vegetation resistance." *J. Hydraul. Eng.*, 116, 691–705.

Swain, E., Wolfert, M., Bales, J., and Goodwin, C. (2004). "Two-dimensional hydrodynamic simulation of surface-water flow and transport to Florida Bay through the Southern Inland and Coastal Systems (SICS)." *Water-Resources Investigations Rep. No. 03-4287*, United States Geological Survey.

Tsihrintzis, V., and Madiedo, E. (2000). "Hydraulic resistance determination in marsh wetlands." *Water Resour. Manage.*, 14, 285–309.

U.S. Army Corps of Engineers. (2008). *Users Guide To RMA2WES Version 4.5.*, US Army, Engineer Research and Development Center Waterways Experiment Station Coastal and Hydraulics Laboratory, Vicksburg, MS.

Variano, E., Ho, D., Engel, V., Schmieder, P., and Reid, M. (2009). "Flow and mixing dynamics in a patterned wetland: Kilometer-scale tracer releases in the Everglades." *Water Resour. Res.*, 45, W08422.

Wang, C., and Wang, P. (2007). "Hydraulic resistance characteristics of riparian reed zone in river." *J. Hydrol. Eng.*, 12(3), 267–272.